OPEN

Photon-Counting Detector CT-Based Vascular Calcium Removal Algorithm

Assessment Using a Cardiac Motion Phantom

Thomas Allmendinger, PhD, Tristan Nowak, PhD,* Thomas Flohr, PhD,*† Ernst Klotz, Dipl Phys,* Junia Hagenauer, Cand. Med.,* Hatem Alkadhi, MD, MPH, EBCR, FESER,§ and Bernhard Schmidt, PhD*‡*

Objectives: The diagnostic performance of coronary computed tomography angiography is known to be negatively affected by the presence of severely calcified plaques in the coronary arteries. In this article, the performance of a novel image reconstruction algorithm (PureLumen) based on spectral CT data of a first-generation dual-source photon-counting detector computed tomography (PCD-CT) system was assessed in a phantom study. PureLumen tries to remove only the calcified contributions from the image while leaving the rest unmodified.

Materials and Methods: The study uses 2 iodine contrast filled vessel phantoms (diameter 4 mm) filled with different concentrations of iodine and equipped with calcified stenosis inserts. Each phantom features 2 separate calcified lesions of 25% and 50% percentage diameter stenosis (PDS) size. The vessel phantoms were mounted inside an anthropomorphic thorax phantom attached to an artificial motion device, simulating realistic cardiac motion at heart rates between 50 beats per minute and 100 beats per minute. Acquisitions were performed using a prospectively electrocardiogram triggered dual-source sequence mode on a PCD-CT system (NAEOTOM Alpha, Siemens Healthineers). Images were reconstructed at 80% of the RR interval with virtual monoenergetic images (Mono) and with additional calcium-removal (PureLumen), both at 65 keV. PureLumen is based on a spectral base material decomposition into iodine and calcium, which aims to reconstruct images without calcium contributions, while leaving all other material contribution unchanged. Stenosis grade was assessed individually for each vessel insert in all reconstructed image series by 2 readers.

Results: The measured median PDS values for the 50% lesion were 56.0% (52.0%, 57.0%) for the Mono case and 50.0% (48.5%, 51.0%) for PureLumen. The 25% lesion median PDS values were 36.0% (29.5%, 39.5%) for Mono and 31.5% (30.5%, 34.0%) for PureLumen. Both lesion sizes demonstrate a significant difference between Mono and PureLumen in their result ($P < 0.05$) with PureLumen median values being closer to the actual true stenosis size for the 50% and 25% lesion. A visual assessment of the image quality depending on the heart rate yielded good image quality up to a heart rate of 80 beats per minute in the PureLumen case.

Conclusions: This phantom study shows that a novel calcium-removal image reconstruction algorithm (PureLumen) using a first-generation dual-source PCD-CT effectively decreases blooming artifacts caused by heavily calcified plaques and improves image interpretability. It also shows that PureLumen retains its performance in the presence of motion with simulated heart rates up to 80 beats per minute. Future in vivo clinical studies are needed to confirm the benefits of this type of reconstruction in terms of coronary computed tomography angiography quality and accuracy.

Key Words: multidetector computed tomography, photon-counting CT, cardiac imaging, spectral imaging, algorithm, blooming, calcium, artifacts

(*Invest Radiol* 2022;57: 399–405)

HIGHLIGHTS

Key finding: Motion phantom-based evaluation of artificial vessels using a dedicated calcium-removal algorithm (PureLumen) effectively decreases blooming artifacts caused by heavily calcified plaques compared with standard virtual monoenergetic images (Mono) reconstructed from first-generation dual-source photon-counting detector computed tomography (PCD-CT).

Importance: The diagnostic performance of coronary computed tomography angiography (CCTA) is known to be hampered by the presence of severely calcified plaques. This is due to blooming artifacts resulting from dense calcification, potentially leading to increased false-positive rates of coronary lumen stenosis.

Noninvasive anatomic assessment by CCTA is applied clinically for the detection and exclusion of significant coronary artery disease for which it shows high diagnostic performance in patients with low to intermediate risk.[1–3] However, as of today, one of the main limitations of coronary CTA imaging is its limited accuracy in the evaluation of calcified lesions.[4–7] Extensive calcifications often lead to an overestimation of the degree of stenosis.[4,6,7] This can be attributed to partial volume averaging of different densities within a single voxel, in combination with some degree of motion artifact. High-density calcifications contaminate the density of other tissues in the voxel and adjacent voxels, which results in blurring of interfaces and an overestimation of calcified lesion size.[8,9] In addition to this, very dense deposits of calcium can cause streak and beam hardening artifacts.

Lately, the first whole-body, dual-source PCD-CT (NAEOTOM Alpha, Siemens Healthineers) was cleared for clinical use. Compared with conventional energy-integrating detectors, in which an indirect conversion technology is used to detect the incident photons, PCD technology uses semiconductors that directly convert x-ray photons to electrical signals.[10–13] The main advantages of PCD-CT are reduced electronic noise, increased contrast-to-noise ratio, improved spatial resolution, and the availability of spectral information in all standard acquisitions.[14–20] The standard reconstruction type of this scanner is Mono, due to the inherent multienergy capabilities of PCD-CT. In addition, it is also possible to generate images using dedicated material decomposition-based algorithms using the multienergy data provided by the PCD-CT system such as iodine and virtual noncontrast.[21]

The goal of this phantom study was the assessment of a spectral PCD-CT data-based image reconstruction algorithm (PureLumen), which omits calcified contributions (calcified lesions, bone, etc) from the final image, while leaving all other material contributions unchanged. This method

Received for publication October 13, 2021; and accepted for publication, after revision, November 11, 2021.

From *Siemens Healthcare GmbH, Forchheim; †University Tübingen, Tübingen; ‡University Erlangen, Erlangen, Germany; and §Institute of Diagnostic and Interventional Radiology, University Hospital Zurich, University of Zurich, Zurich, Switzerland.

Conflicts of interest and sources of funding: none declared. T.A., T.N., T.F., E.K., J.H., and B.S. are employees of Siemens Healthcare GmbH.

Correspondence to: Thomas Allmendinger, PhD, Siemens Healthcare GmbH, Siemens Strasse 3, 91301 Forchheim, Germany. E-mail: thomas.allmendinger@siemens-healthineers.com.

ISSN: 0020-9996/22/5706–0399
DOI: 10.1097/RLI.0000000000000853

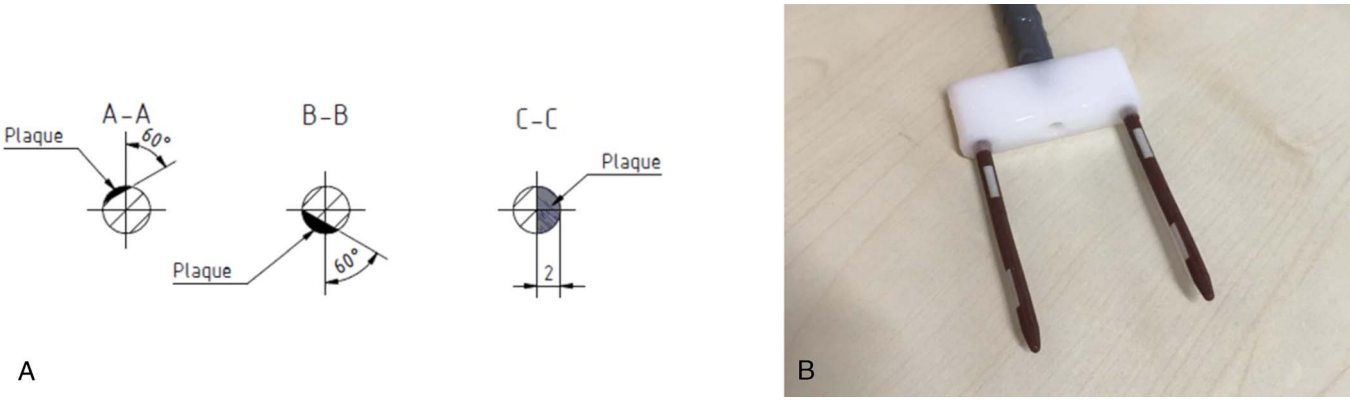

FIGURE 1. A, Cross-sectional drawing of the artificial vessel with 4 mm diameter containing 3 calcified lesions (QRM, Moehrendorf, Germany). The calcified lesions were manufactured to contain 800 mg/mL hydroxyapatite. B, Photograph of the carrier mounted vessels with the calcified lesions clearly visible. The mounting on the same carrier enabled simultaneous measurement in the cardiac motion phantom.

attempts to improve accuracy in terms of remaining vessel lumen and stenosis evaluation by preventing the negative calcium blooming effects due to the suppression of calcium material.

The study was based on phantom measurements of 2 artificial coronary vessels with different iodine vessel contrast and embedded calcified lesions. These vessels were measured in a cardiac motion phantom at different heart rates up to 100 beats per minute to provide a realistic environment for a CCTA examination. The focus of the study was on testing an advanced spectral algorithm under the increasingly difficult situation generated by the phantom motion toward higher heart rates. Existing literature in this context is often limited to a static evaluation or a simple spectral postprocessing.[22,23]

MATERIALS AND METHODS

Vessel Phantom

Two custom-built vessel phantoms (QRM, Moehrendorf, Germany) with 4 mm diameter and calcified lesions, as shown in Figure 1, were used. Each phantom consisted of a solid cylinder of compound mimicking a mixture of blood and iodine contrast with a CT value of 500 HU or 800 HU, respectively, on a standard energy-integrating CT system at a tube voltage of 120 kV. Along the main axis of each phantom, and arranged at different angles, 3 solid artificial calcified lesions with a hydroxyapatite concentration of 800 mg/mL were placed as straight cylinder segments cut parallel to the rotational axis, each with a length of 10 mm and an intermittent space of 5 mm. The calcified lesions realized a CT value of 1100 HU on a standard energy-integrating CT system at a tube voltage of 120 kV. In perpendicular vessel cuts, the 3 calcifications were engineered to generate diameter stenosis of 12.5%, 25%, and 50% relative to the vessel diameter of 4 mm.

Motion Phantom

A semianthropomorphic thorax CT phantom and a 4D coronary motion simulator (Cardio CT Phantom and Sim4DCardio; QRM, Moehrendorf, Germany) were used (Fig. 2). The cardiac phantom simulated the thorax of a medium-sized patient with respect to the attenuation characteristics. The dimensions of the phantom along the *x*, *y*, and *z* axis were 20 cm, 30 cm, and 10 cm, respectively. It contained artificial lungs and a spine insert that was surrounded by soft tissue equivalent material. The artificial vessels were attached to a carrier, which was itself attached to the motion phantom, and placed inside a water tank with 10 cm diameter, which was inserted into the thorax phantom. The coronary motion simulator enabled computer controlled short range motion trajectories in 3D (*x*, *y*, and *z* axis), mimicking the natural motion of the coronary arteries. The motion amplitudes are in the order of 2 mm in plane and 3 mm out of plane. The 4D coronary motion simulator was set in an electrocardiogram (ECG) synchronized fashion and provided an artificial ECG signal to the CT system with heart rates

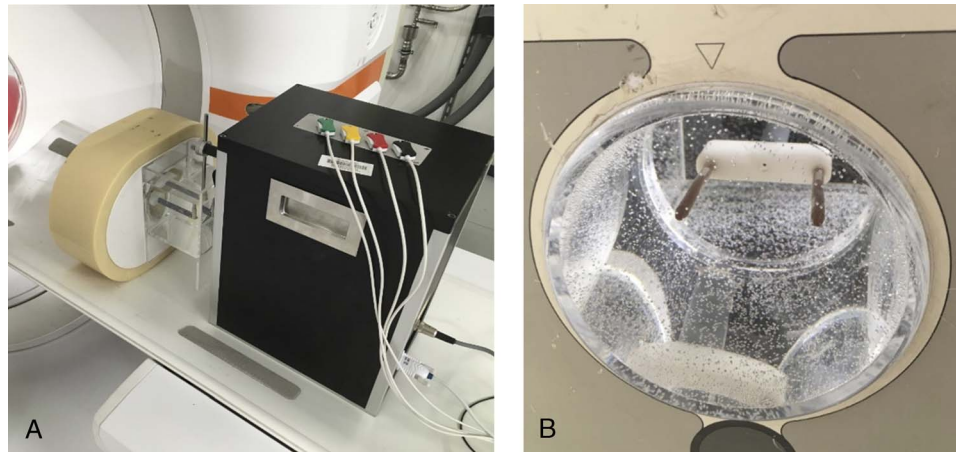

FIGURE 2. Photographs of the thorax CT semianthropomorphic phantom (A), and the 4D coronary motion simulator (B), (Cardio CT Phantom and Sim4DCardio; QRM, Forchheim, Germany). The 4D simulator was assembled with both 4 mm artificial vessels at the same time.

between 50 beats per minute and 100 beats per minute. The applied motion profiles were provided by the manufacturer and were derived from clinical coronary vessel velocity profiles originally obtained from electron-beam CT data.[24]

Scanning and Reconstruction

All acquisitions were performed using a prospectively ECG triggered dual-source sequential mode on a first-generation dual-source PCD-CT system. Tube voltage was set to 120 kV, which is a prerequisite for the application of the calcium removal algorithm, and automatic tube current modulation was enabled with a quality reference IQ level of 150. Scan length was set to 10.5 cm with a detector collimation of 138 × 0.4 mm, an acquisition consisting of 2 sequence steps. Gantry rotation time was set to 0.25 seconds time, and the ECG target phase was set to 80%. To cover a realistic range of motion patterns, a single acquisition was performed with activated motion for each heart rate at 60, 80, and 100 beats per minute. The $CTDI_{vol}$ values were 17.7 mGy for all heart rates. These acquisitions were evaluated in a quantitative manner and were therefore performed at a higher diagnostic image quality level.

All reconstructions were done at a fixed phase of 80% with a temporal resolution of 66 milliseconds in all images. The selected 80% phase represents the expected state of minimal vessel motion derived from the theoretical coronary simulator motion profiles.[24] Reconstructions were performed as traditional Mono and as calcium-removed images (PureLumen) at an energy of 65 keV, which is equivalent to the mean energy of the 120 kV acquisition spectra. All other reconstruction parameters were matched in all series with slice thickness of 0.6 mm and increment of 0.4 mm, field of view of 150 mm, and vascular reconstruction kernel Bv44 with iterative reconstruction strength 3 (QIR or quantum iterative reconstruction).

A separate set of measurements was acquired without motion and at heart rates between 50 and 100 beats per minute in steps of 10 beats per minute at an IQ level of 75 for a dedicated visual assessment at a more clinically used diagnostic image quality level. The $CTDI_{vol}$ values for these measurements were 8.8 mGy for all heart rates. These measurements were reconstructed with a slightly softer kernel Bv40 to account for the increased noise level with all other settings unchanged.

Algorithm Description "PureLumen"

The aim of the PureLumen algorithm is the reconstruction of images, which omit all contributions from calcium or bone-like material from the final image, while leaving all other material values unchanged with respect to their HU values, similar to a method described in Mannil et al.[25] The algorithm is based on spectrally resolved multithreshold PCD-CT data, which enables a material decomposition into different types of base materials. This principle has been established for quite some time[26,27]; a more recent discussion on the synthetization of Mono as an example of a spectrally resolved CT algorithm is found in Yu et al[28] and Grant et al.[29]

The algorithmic flow of PureLumen can be broken into 4 main blocks, followed by a final fusing. They are shown in Figure 3 labeled "calcium mapping," "soft-tissue offset," "iodine/calcium base decomposition," and "monoenergetic keV generation."

"Monoenergetic keV generation" describes the synthetization of a standard Mono that will be used for the final blending step. The actual keV setting and its iterative reconstruction strength is specified by the user; therefore, this image is identical to a standard Mono image with identical input settings.

"Iodine/calcium base decomposition" describes the synthetization of a "noncalcium" image based on suitable PCD-CT specific tabulated spectral material parameters for iodine and calcium base materials. The notion "noncalcium" image instead of "iodine" image is more suitable at this point as it contains all material contributions but omits calcium components.

"Calcium mapping" uses the spectral information derived from iodine and calcium material decomposition into a calcium image map.

The "soft-tissue offset" block feeds into the "iodine/calcium base decomposition" part based on a standard virtual noncontrast image. This offset calculation is used in the decomposition process to ensure that materials, which are spectrally significantly different from calcium and iodine (eg, air or fat), are excluded, because these would otherwise be decomposed into nonphysical HU values.

The final reconstruction step consists of a blending operation of the Mono and the iodine image using the calcium map as weighting image.

Vessel Lumen Evaluation

A quantitative analysis was performed for the 25% and 50% lesions. The 12.5% calcified stenosis was not evaluated due to the lack of clinical relevance. In each of the 4 different calcified lesion inserts in each reconstruction, the remaining vessel lumen diameter was measured in millimeters at 3 different positions within the lesion in images oriented axial with respect to the vessel axis in a standard viewer application (RadiAnt DICOM Viewer 2021.1). In accordance with clinical practice,[30] the lumen diameter of the unobstructed lumen was also measured proximal and distal of the lesion in millimeter. A synchronized coronal view served as guide for identifying suitable measurements positions for each lesion. The percentage diameter stenosis (PDS) value is derived from these measurements by calculating an average of the unobstructed vessel values D_V and a separate average of the remaining lumen within the lesion D_L yielding the PDS value as $1–D_L/D_V$. To suppress the influence of window-level settings, matching settings were

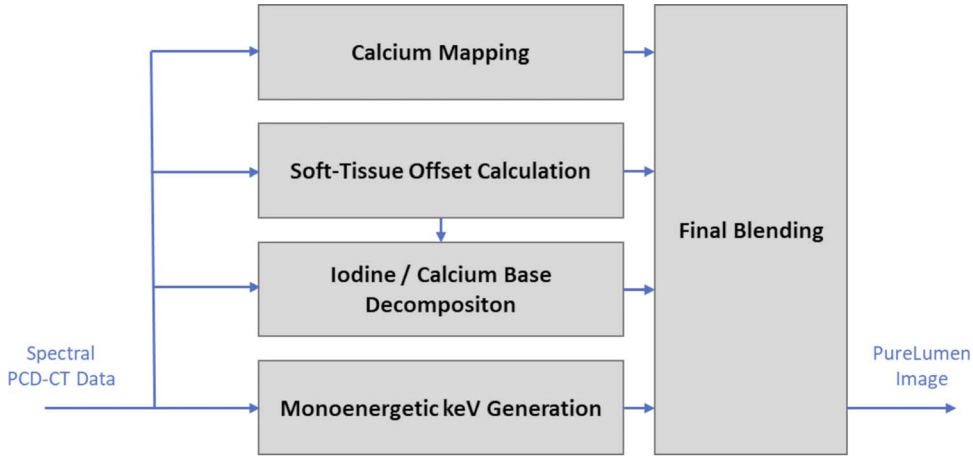

FIGURE 3. Simplified flow chart illustrating the PureLumen algorithm and image reconstruction.

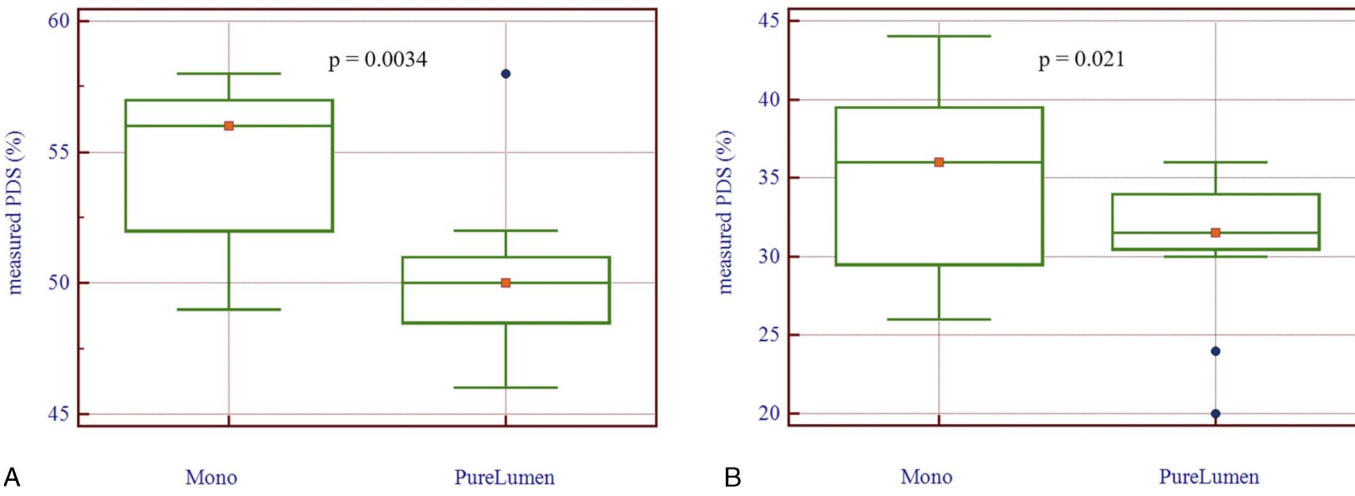

FIGURE 4. Comparison of measured percent diameter stenosis (PDS) values for the Mono and PureLumen reconstructions: (A) 50% nominal stenosis, (B) 25% nominal stenosis. The *P* values are from a paired Wilcoxon test.

used on the Mono and PureLumen reconstructions, individually for the 2 vessel phantoms.

Measurements were performed independently by 2 readers with more than 10 years' experience in the field. Both measurements were included individually in the evaluation in a pooled fashion.

A visual assessment of the image quality for the Mono and PureLumen reconstruction was performed on the separately acquired data set with lower image quality IQ level of 75. Images were reformatted parallel to the phantom axis and orthogonally to the calcium lumen interface similar to curved MPRs used in clinical reading.

Statistical Analysis

Statistical analysis was performed using MedCalc Statistical Software.[31] Percentage diameter stenosis values are expressed as medians with interquartile range (IQR). The differences between Mono and PureLumen PDS were assessed by box and whisker plots and paired Wilcoxon test. Reader agreement was assessed by correlation analysis and Bland-Altman plots. In addition, 95% confidence intervals were calculated. A 2-tailed *P* value of less than 0.05 was considered statistically significant.

RESULTS

The measured PDS values for the 50% lesion were 56.0% (IQR, 52.0%–57.0%) for Mono and 50.0% (IQR, 48.5%–51.0%) for PureLumen. The 25% lesion PDS values were 36.0% (IQR, 29.5%–39.5%) for Mono and 31.5% (IQR, 30.5%–34.0%) for PureLumen. An illustration in the form of paired box and whisker plots is shown in Figure 4.

For the 50% lesion, the PureLumen result was identical to the nominal 50% stenosis value, the IQR over the variation of phantom and scan settings was only half of the Mono result (2.5% vs 5.0%), and the difference with a *P* value of 0.0034 was significant.

For the 25% lesion, the PureLumen result was closer to the nominal value, the IQR was also reduced from 10% to 5.5%, and the improvement with a *P* value of 0.021 remained significant.

Reader agreement on all measurements was high. Percentage diameter stenosis readings correlated with a correlation coefficient of 0.94 ($P < 0.001$). Separate Bland-Altman analysis of Mono and PureLumen PDS values showed a small reduction of interreader variability. Mono readings differed by 5.1% (95% confidence intervals [CIs], 1.8%–8.3%) with limits of agreement between −4.9% and 15.1%. For the PureLumen reconstructions, the difference was 2.2% (95% CI, −0.7% to 5.0%) with limits of agreement between −6.6% and 10.9%.

Figure 5 provides example images at 65 keV of the 50% (left) and 25% (right) lesion for 1 of the vessels at a heart rate of 60 beats per minute. In comparison to the Mono reconstruction (top row), an improved visualization of the vessel lumen is depicted in the PureLumen reconstruction (bottom row), not affected by the potential overestimation from calcium blooming based on reconstructions taken at the IQ 150 level. All images shown are matched in terms of their axial slice position in the middle of the 50% and 25% lesion and their window level settings (C300/W1100).

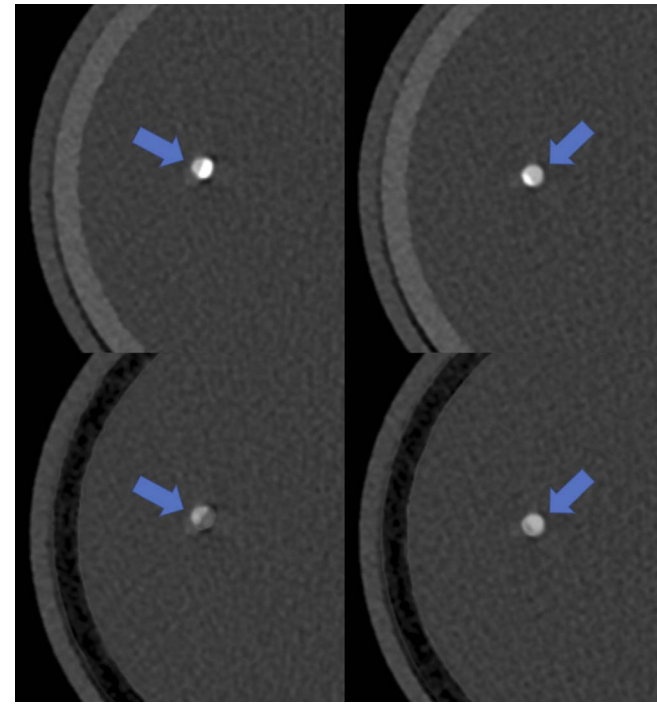

FIGURE 5. Axial example images at 65 keV of the 50% (left) and 25% (right) lesion for one of the vessels at a heart rate of 60 beats per minute. In comparison to the Mono reconstruction (top row), an improved visualization of the vessel lumen is depicted in the PureLumen reconstruction (bottom row), not affected by the potential overestimation from calcium blooming (lumen indicated by blue arrows).

Figure 6 illustrates the effects of an increasing heart rate for the vessel phantom with 500 HU nominal iodine enhancement for Mono and PureLumen without motion and at heart rates between 50 beats per minute and 100 beats per minute in steps of 10 beats per minute.

Visual inspection of these images taken at the reduced IQ level of 75 shows a considerable calcium blooming effect for both 50% and 25% lesions in the Mono case with a slight increase of the effect toward higher heart rates. Qualitative assessment demonstrates good PureLumen image quality results for the 50% lesions up to a heart rate of approximately 80 beats per minute. A reduction of the quality is observed for PureLumen at 90 beats per minute and 100 beats per minute, whereas for the Mono case, the increase in motion artifacts seems to be milder. The PureLumen pattern for the small 25% lesion (Fig. 6) seems to be more variable. This might also explain why there were 2 negative outliers in the quantitative measurements (Fig. 4B).

This supports the notion that visual scoring probably becomes more reliable when both reconstructions, standard mono and PureLumen, are jointly considered for the interpretation.

DISCUSSION

One of the main limitations of coronary CTA imaging is its reduced accuracy in the evaluation of stenosis in the presence of calcified lesions.[4–7] High-density calcifications may lead to an overestimation of the degree of stenosis,[4,6,7] which can be attributed to partial volume averaging because of blurring of interfaces and an overestimation of calcified lesion size.[8] Blooming artifacts can be reduced by increasing spatial resolution through thin slice reconstruction, as well as use of sharper reconstruction kernels. However, these approaches come at the expense of higher image noise or higher radiation dose requirements for suppressing image noise. This phantom study suggests that a novel calcium-removal image reconstruction algorithm (PureLumen) using a first-generation dual-source PCD-CT decreases blooming artifacts caused by heavily calcified plaques and improves image interpretability. This can be seen in the measured PDS values for the nominal 50% lesion, which overestimates the stenosis in the Mono case with 56.0% (52.0%–57.0%) compared with the result compatible with the lesion size in the PureLumen case with 50.0% (IQR, 48.5%–51.0%). In case of the small lesion, a similar overestimation of the Mono reconstruction was seen with 36.0% (IQR, 29.5%–39.5%), which was significantly reduced in the PureLumen case to 31.5% (IQR, 30.5%–34.0%). A small overestimation of the nominal 25% lesion value remained also in the PureLumen reconstruction, which might not be relevant because calcified lesions below 30% diameter reduction are of limited clinical significance.[32] In both cases, a reduction of the IQR from 5% down to 2.5% for the 50% lesion and from 10% to 5.5% in the 25% lesion between Mono and PureLumen suggests a more consistent stenosis estimation. From a utilization point of view, it is therefore suggested to use the PureLumen reconstruction as additional source of information in CCTA examinations besides a standard monoenergetic reconstruction in cases of heavy calcifications.

In all PDS measurements, an overall high reader agreement was observed (correlation coefficient of 0.94, $P < 0.001$). Bland-Altman analysis of Mono and PureLumen PDS values showed a small reduction of interreader variability. Mono readings differed by 5.1% (95% CI, 1.8%–8.3%) with limits of agreement between −4.9% and 15.1%. For the PureLumen reconstructions, the difference was 2.2% (95% CI, −0.7% to 5.0%) with narrow limits of agreement between −6.6% and 10.9%. This result for the standard Mono images is compatible with findings in a large-scale clinical trial study, which showed increased reader discordance between site and core laboratory CCTA interpretations at

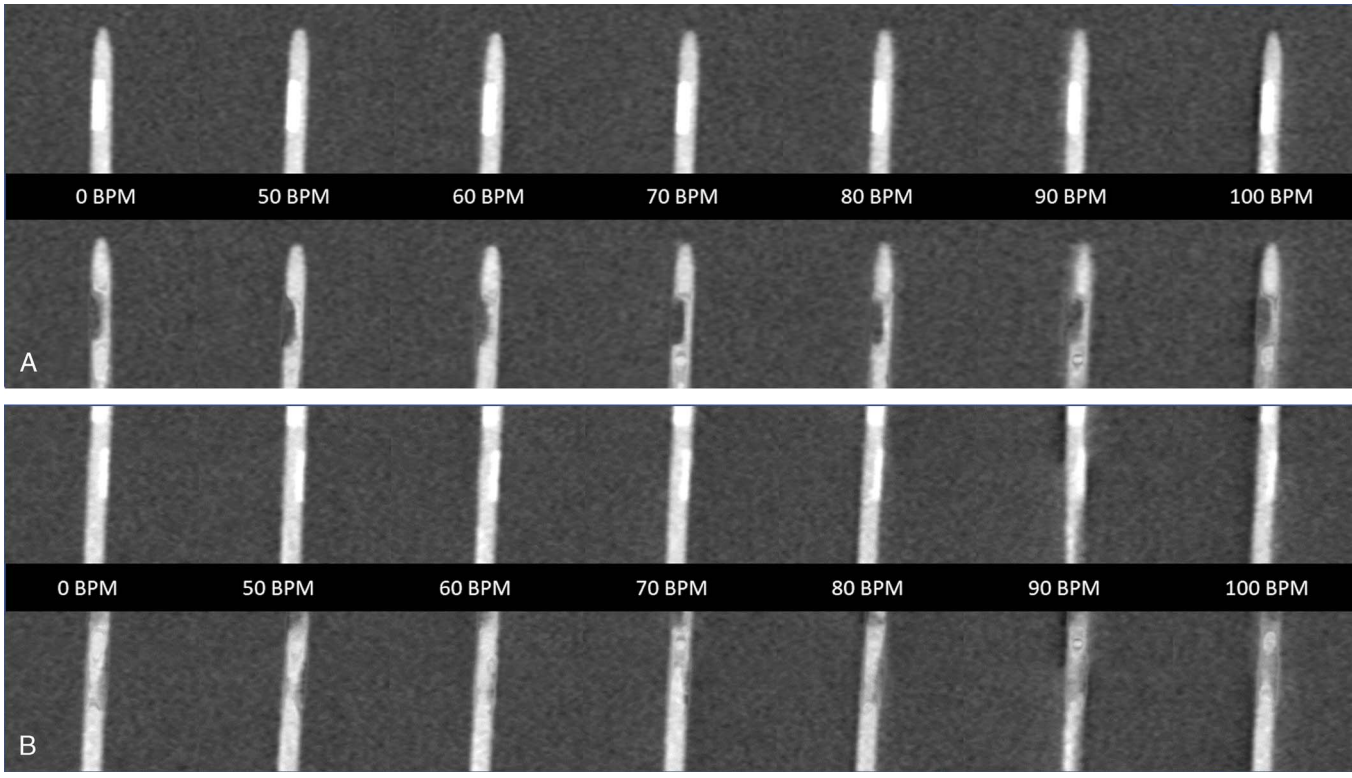

FIGURE 6. Longitudinal multiplanar reconstructions orthogonal to the vessel stenosis of the 50% lesion (A) and 25% lesion (B) for the standard Mono (top row) and PureLumen (bottom row) case. The individual tiles from left to right illustrate the different heart rates from "at rest" to up to 100 b (left to right). The window level is identical in all images (C300/W900).

increasing calcium scoring categories[33] and therefore in the presence of heavy calcifications.

Visual assessment of the heart rate dependency derived from the images taken at the reduced IQ level of 75 showed good PureLumen image quality results over a wide range of heart rates. However, PureLumen seemed to reach the limits of acceptable image quality at slightly lower heart rates compared with the standard Mono reconstruction. Nevertheless, the potential benefits of a PureLumen reconstruction can be seen in the visual assessment of stenosis grades for heavily calcified plaques as a considerable amount of calcium blooming was present and a considerable overestimation of the stenosis grade could have been expected for the 50% and the 25% lesion case if only the Mono images would have been provided. One might argue that both reconstructions provide complementary information, and that a stenosis evaluation in a clinical setting should be based on images presented in a synchronized side-by-side fashion.

Our study has several limitations. First, this was a phantom study with inherent limitations, primarily only 2 distinct artificial vessel samples with different iodine concentrations were examined. Variations in terms of lumen diameter and calcium concentration were therefore omitted as well as the bias, which is introduced by the fact that the lesions were cut "geometrically" with a well-defined shape. The size distribution of the lesions was also not ideal for CCTA considerations, and a high-grade 75% stenosis would have been better suited. In addition, the acquisitions for the quantitative evaluation were performed at an elevated image quality dose level compared with a clinical setting to minimize the influence of statistical effects, which would otherwise be introduced in the comparisons between the 2 reconstruction methods. However, as the additional qualitative assessment at a relative standard IQ level demonstrates, this does not seem to be a major limitation. Another potential limitation is the prerequisite of a 120-kV acquisition for the PureLumen algorithm itself, which might result in elevated dose values in clinical practice compared with the established low-kV approach in CCTA imaging.[34] Therefore, the main aim of this study was the demonstration of the technical feasibility of a calcium-removal algorithm in a coronary CTA mimicking environment, including ECG triggering, gated reconstruction, and realistic coronary motion applied to artificial coronary vessel phantoms. A key element of the study setup was the inclusion of coronary motion over a wide range of heart rates up to 100 beats per minute, which tends to be ignored in phantom-based studies, as motion is often the primary concern in CCTA examinations.[8] Future in vivo studies are required to clarify, whether the positive effects in terms of calcium blooming reduction and stenosis quantification for the PureLumen case can be transferred into improved CCTA quality in vivo and ultimately into improved patient outcome.

CONCLUSIONS

This technical feasibility study using a cardiac motion phantom shows that a novel calcium-removal image reconstruction algorithm (PureLumen) using a first-generation dual-source PCD-CT seems to generate images with good quality in the presence of motion for a wide range of heart rates and effectively decreases blooming artifacts caused by heavily calcified plaques. It also improves image interpretability and might reduce reader discordance. Future clinical studies in vivo are needed to confirm the benefits of this type of reconstruction in terms of CCTA quality and accuracy.

REFERENCES

1. Meijboom WB, Meijs MF, Schuijf JD, et al. Diagnostic accuracy of 64-slice computed tomography coronary angiography: a prospective, multicenter, multivendor study. *J Am Coll Cardiol*. 2008;52:2135–2144. doi:10.1016/j.jacc.2008.08.058.
2. Budoff MJ, Dowe D, Jollis JG, et al. Diagnostic performance of 64-multidetector row coronary computed tomographic angiography for evaluation of coronary artery stenosis in individuals without known coronary artery disease: results from the prospective multicenter ACCURACY (assessment by coronary computed tomographic angiography of individuals undergoing invasive coronary angiography) trial. *J Am Coll Cardiol*. 2008;52:1724–1732. doi:10.1016/j.jacc.2008.07.031.
3. Hulten EA, Carbonaro S, Petrillo SP, et al. Prognostic value of cardiac computed tomography angiography: a systematic review and meta-analysis. *J Am Coll Cardiol*. 2011;57:1237–1247. doi:10.1016/j.jacc.2010.10.011.
4. Zhang S, Levin DC, Halpern EJ, et al. Accuracy of MDCT in assessing the degree of stenosis caused by calcified coronary artery plaques. *AJR Am J Roentgenol*. 2008;191:1676–1683. doi:10.2214/AJR.07.4026.
5. Raff GL, Gallagher MJ, O'Neill WW, et al. Diagnostic accuracy of noninvasive coronary angiography using 64-slice spiral computed tomography. *J Am Coll Cardiol*. 2005;46:552–557. doi:10.1016/j.jacc.2005.05.056.
6. Hoffmann U, Moselewski F, Cury RC, et al. Predictive value of 16-slice multidetector spiral computed tomography to detect significant obstructive coronary artery disease in patients at high risk for coronary artery disease: patient-versus segment-based analysis. *Circulation*. 2004;110:2638–2643. doi:10.1161/01.CIR.0000145614.07427.9F.
7. Vavere AL, Arbab-Zadeh A, Rochitte CE, et al. Coronary artery stenoses: accuracy of 64-detector row CT angiography in segments with mild, moderate, or severe calcification—a subanalysis of the CORE-64 trial. *Radiology*. 2011;261:100–108. doi:10.1148/radiol.11110537.
8. Kalisz K, Buethe J, Saboo SS, et al. Artifacts at cardiac CT: physics and solutions. *Radiographics*. 2016;36:2064–2083. doi:10.1148/rg.2016160079.
9. Renker M, Nance JW, Schoepf UJ, et al. Evaluation of heavily calcified vessels with coronary CT angiography: comparison of iterative and filtered back projection image reconstruction. *Radiology*. 2011;260:390–399. doi:10.1148/radiol.11103574.
10. Alkadhi H, Euler A. The future of computed tomography: personalized, functional, and precise. *Invest Radiol*. 2020;55:545–555. doi:10.1097/RLI.0000000000000066811.
11. Flohr T, Petersilka M, Henning A, et al. Photon-counting CT review. *Phys Med*. 2020;79:126–136. doi:10.1016/j.ejmp.2020.10.030.
12. Willemink MJ, Persson M, Pourmorteza A, et al. Photon-counting CT: technical principles and clinical prospects. *Radiology*. 2018;289:293–312. doi:10.1148/radiol.2018172656.
13. Hsieh SS, Leng S, Rajendran K, et al. Photon counting CT: clinical applications and future developments. *IEEE Trans Radiat Plasma Med Sci*. 2021;5:441–452. doi:10.1109/trpms.2020.3020212.
14. Euler A, Higashigaito K, Mergen V, et al. High-pitch photon-counting detector computed tomography angiography of the aorta: intraindividual comparison to energy-integrating detector computed tomography at equal radiation dose. *Invest Radiol*. 2021. doi:10.1097/RLI.0000000000000816.
15. Sandstedt M, Marsh J Jr., Rajendran K, et al. Improved coronary calcification quantification using photon-counting-detector CT: an ex vivo study in cadaveric specimens. *Eur Radiol*. 2021;31:6621–6630. doi:10.1007/s00330-021-07780-6.
16. Eberhard M, Mergen V, Higashigaito K, et al. Coronary calcium scoring with first generation dual-source photon-counting CT-first evidence from phantom and in-vivo scans. *Diagnostics (Basel)*. 2021;11:1708. doi:10.3390/diagnostics11091708.
17. Jungblut L, Blüthgen C, Polacin M, et al. First performance evaluation of an artificial intelligence-based computer-aided detection system for pulmonary nodule evaluation in dual-source photon-counting detector CT at different low-dose levels. *Invest Radiol*. 2021. doi:10.1097/rli.0000000000000814.
18. Sartoretti T, Eberhard M, Nowak T, et al. Photon-counting multienergy computed tomography with spectrally optimized contrast media for plaque removal and stenosis assessment. *Invest Radiol*. 2021;56:563–570. doi:10.1097/rli.0000000000000773.
19. Higashigaito K, Euler A, Eberhard M, et al. Contrast-enhanced abdominal CT with clinical photon-counting detector CT: assessment of image quality and comparison with energy-integrating detector CT. *Acad Radiol*. 2021;S1076-6332(21)00305–6. doi:10.1016/j.acra.2021.06.018.
20. Petritsch B, Petri N, Weng AM, et al. Photon-counting computed tomography for coronary stent imaging: in vitro evaluation of 28 coronary stents. *Invest Radiol*. 2021;56:653–660. doi:10.1097/RLI.0000000000000787.
21. Johnson TR, Krauss B, Sedlmair M, et al. Material differentiation by dual energy CT: initial experience. *Eur Radiol*. 2007;17:1510–1517. doi:10.1007/s00330-006-0517-6.
22. Jin KN, Chung JW, Park EA, et al. Dual-energy computed tomography angiography: virtual calcified plaque subtraction in a vascular phantom. *Acta Radiol Open*. 2017;6:2058460117717765. doi:10.1177/2058460117717765.
23. Boll DT, Merkle EM, Paulson EK, et al. Calcified vascular plaque specimens: assessment with cardiac dual-energy multidetector CT in anthropomorphically moving heart phantom. *Radiology*. 2008;249:119–126. doi:10.1148/radiol.2483071576.
24. Achenbach S, Ropers D, Holle J, et al. In-plane coronary arterial motion velocity: measurement with electron-beam CT. *Radiology*. 2000;216:457–463. doi:10.1148/radiology.216.2.r00au19457.
25. Mannil M, Ramachandran J, Vittoria de Martini I, et al. Modified dual-energy algorithm for calcified plaque removal: evaluation in carotid computed tomography angiography and comparison with digital subtraction angiography. *Invest Radiol*. 2017;52:680–685. doi:10.1097/RLI.0000000000000391.

26. Alvarez RE, Macovski A. Energy-selective reconstructions in x-ray computerized tomography. *Phys Med Biol*. 1976;21:733–744. doi:10.1088/0031-9155/21/5/002.
27. Lehmann LA, Alvarez RE, Macovski A, et al. Generalized image combinations in dual KVP digital radiography. *Med Phys*. 1981;8:659–667. doi:10.1118/1.595025.
28. Yu L, Leng S, McCollough CH. Dual-energy CT-based monochromatic imaging. *AJR Am J Roentgenol*. 2012;199(suppl 5):S9–S15. doi:10.2214/AJR.12.9121.
29. Grant KL, Flohr TG, Krauss B, et al. Assessment of an advanced image-based technique to calculate virtual monoenergetic computed tomographic images from a dual-energy examination to improve contrast-to-noise ratio in examinations using iodinated contrast media. *Invest Radiol*. 2014;49:586–592. doi:10.1097/RLI.0000000000000060.
30. Arbab-Zadeh A, Hoe J. Quantification of coronary arterial stenoses by multidetector CT angiography in comparison with conventional angiography methods, caveats, and implications. *JACC Cardiovasc Imaging*. 2011;4:191–202. doi:10.1016/j.jcmg.2010.10.011.
31. MedCalc Statistical Software version 19.2.6, MedCalc Software Ltd. Ostend Belgium.
32. Cury RC, Abbara S, Achenbach S, et al. CAD-RADS(TM) coronary artery disease - reporting and data system. An expert consensus document of the Society of Cardiovascular Computed Tomography (SCCT), the American College of Radiology (ACR) and the north American Society for Cardiovascular Imaging (NASCI). Endorsed by the American College of Cardiology. *J Cardiovasc Comput Tomogr*. 2016;10:269–281. doi:10.1016/j.jcct.2016.04.005.
33. Lu MT, Meyersohn NM, Mayrhofer T, et al. Central core laboratory versus site interpretation of coronary CT angiography: agreement and association with cardiovascular events in the PROMISE trial. *Radiology*. 2018;287:87–95. doi:10.1148/radiol.2017172181.
34. Abbara S, Blanke P, Maroules CD, et al. SCCT guidelines for the performance and acquisition of coronary computed tomographic angiography: a report of the Society of Cardiovascular Computed Tomography Guidelines Committee: endorsed by the North American Society for Cardiovascular Imaging (NASCI). *J Cardiovasc Comput Tomogr*. 2016;10:435–449. doi:10.1016/j.jcct.2016.10.002.